

by a simple impedance. The resistance that dominates the system impedance is higher in the low pressure system than the one observed in the high pressure system. Indeed, the high pressure air flow control system maintains the oxygen utilization during current density increments by operating on increased supply manifold pressure and thus moving between different polarization curves. The closed loop voltage observed, stays consequently almost constant during current changes. The pressure variations in the low pressure system are however very small, so a single polarization curve is used and the system impedance has the resistance of the open loop FC voltage-current circuit.

In summary, it is shown that the dynamic characteristics of the two systems (low pressure blower-based and high pressure compressor-based) are distinct and their limits in transient response arise from different subsystem interaction.

2 Preliminaries on FC air supply system

A brief summary of the FC model with emphasis on the subsystems with the supply manifold pressure (p_{sm}) as the crucial parameter is presented. We then analyze the transient control authority and steady-state capabilities of low and high pressure flow devices such as blowers and compressors. The analysis is based on the high pressure FC stack model in [8] and its low pressure modification. It is assumed that the hydrogen supply system is relatively fast and the hydrogen flow rate can be instantaneously adjusted to provide minimum pressure difference across the membrane. For simplicity, we refer to the FC stack pressure (p_{st}) which is equal to the FC anode and cathode pressure. The relative humidity of the stack inlet hydrogen and air flow is assumed to be 100%. The heat transfer effects are ignored and the temperature of the reactant flows and fuel cell stack are assumed constant at 80°C.

The blower and the compressor are sized so that the excess oxygen ratio λ is equal to 2, where

$$\lambda = \frac{\text{supplied rate of } O_2}{\text{reacted rate of } O_2} \quad (1)$$

The FC stack with 381 cells running at an average of 0.6 V/cell would produce about 330 A and consume approximately 252 m³/hr Air (4200 slm). High stack operating pressure assures air flow, in right proportions, in all the cathode's plates tiny channels. In addition, it improves the reaction rates, and thus, the fuel cells efficiency. Finally, it allows to reach a mass flow rate range of 0 to 0.1 kg/s despite very small dimensions of orifices. The compressor in [8] operates in a range of pressure from 1 to 4 bars.

On the other hand, the compressor needs a lot of power: 10 to 14 kW. This power is taken from the power produced by the fuel cell stack, and thus, decreases the net power actually available to propel the vehicle. The fact that the compressor is an expensive device and operates at a very high and reliability thrilling speed (around 100 kRPM) makes one wonder if it would not be better to use a cheaper and slower device such as blower to provide the air flow. Even though the FC efficiency is lower, lesser power is used to run the blower. A simple blower operates at low speed (a few thousands RPM) and very low pressure (close to the atmospheric pressure) and provides an equivalent range of mass flow rate. In this paper, we create

a model of blower, replace the high pressure compressor model by the blower model, tune and resize the system, and compare the open loop and closed loop behavior of the two fuel cell systems.

3 State Equations

The supply manifold (SM) model represents one lumped volume of all pipes and connections between the flow device and the FC stack. The pressure in the supply manifold, p_{sm} , is governed by mass continuity equation and energy conservation

$$\frac{dm_{sm}}{dt} = W_{fd} - W_{sm} \quad (2)$$

$$\frac{dp_{sm}}{dt} = \frac{\gamma R_a}{V_{sm}} (W_{fd} T_{fd} - W_{sm} T_{sm}) \quad (3)$$

where $R_a = 286.9 \text{ J/(kg}\cdot\text{K)}$ is the air gas constant, $V_{sm} = 0.02 \text{ m}^3$ is the supply manifold volume and T_{sm} is the temperature of the flow inside the manifold which is calculated from the ideal gas law and the two states (m_{sm} and p_{sm}). The supply manifold exit flow, $W_{sm}(p_{sm}, p_{st})$, is calculated using a linearized nozzle flow equation (Eqn. (9)). The inlet flow W_{fd} , which is either the flow of the high speed/pressure compressor W_{cp} or the flow of the low speed/pressure blower W_{bl} , is defined in the next section.

A lumped rotational parameter model with inertia, J , is used to represent the dynamic behavior of the rotational speed of the flow device, ω .

$$J \frac{d\omega}{dt} = (\tau_m - \tau_{fd}) \quad (4)$$

where $\tau_m(v_m, \omega)$ is the motor torque and τ_{fd} is the required torque from the flow device. The motor torque is a function of the motor power input, P_m , and the speed, ω : $\tau_m = \frac{P_m}{\omega}$. The required torque of the flow device $\tau_{fd} = P_{fd}/\omega$ where the required power, P_{fd} , is calculated using thermodynamic equation

$$P_{fd} = C_p \frac{T_{atm}}{\eta_{fd}} \left[\left(\frac{p_{sm}}{p_{atm}} \right)^{\frac{\gamma-1}{\gamma}} - 1 \right] W_{fd} \quad (5)$$

where γ is the air specific heat ratio, C_p is air specific heat, η_m is compressor efficiency, p_{sm} is pressure inside the supply manifold and p_{atm} and T_{atm} are atmospheric pressure and temperature, respectively. Thermodynamic equations are used to calculate the air temperature leaving the flow device, T_{fd} :

$$T_{fd} = T_{atm} + \frac{T_{atm}}{\eta_{cp}} \left[\left(\frac{p_{sm}}{p_{atm}} \right)^{\frac{\gamma-1}{\gamma}} - 1 \right] \quad (6)$$

In the LP system, $\frac{p_{sm}}{p_{atm}} \approx 1$ and thus, $T_{fd} \approx T_{atm} \approx T_{sm}$. Therefore Equations (2) and (3) are linearly dependent and one of them can be eliminated. The LP system can, thus, be represented by two state equations:

$$\frac{dp_{sm}}{dt} = \frac{R_a T_{sm}}{V_{sm}} (W_{fd} - W_{sm}) \quad (7)$$

and (4), whereas, the HP system requires three state equations: (2)-(4).

4 Flow Equations

A static compressor map is used in [8] to determine the air flow rate through the compressor, W_{cp} . The compressor flow characteristic $W_{cp}(p_{sm}/p_{atm}, \omega_{cp})$ is from an Allied Signal compressor [3]. The map is modeled using the Jensen & Kristensen nonlinear curve fitting method [6] and the fitting result is presented in [8].

Due to the high flow rate requirement, a centrifugal blower is selected for the LP FC system. We choose the D1G133-DC13-52 from ebm Industries because there are enough information and data on the German ebm's website to build the model. It is a Dual Inlet blower of which the flow enters from both radial sides of the blower. The rotation of the impeller is obtained from an integrated 24 V DC Motor (M1G074-CF). The motor speed is controlled by changing the input voltage in a range from 16 V to 28 V. The maximum flow rate seems to be around 900 m³/h (0.3 kg/s), the maximum differential pressure is 450 Pa, and the maximum speed 2500 rpm. Figure 2 shows the values of the flow rate, V , the differential pressure, Δp_f , the motor power, P_1 , the operating speeds, n , and the efficiency, $\eta\%$, for 10 different points based on three different voltage, v_m , inputs. We use the Fan Laws:

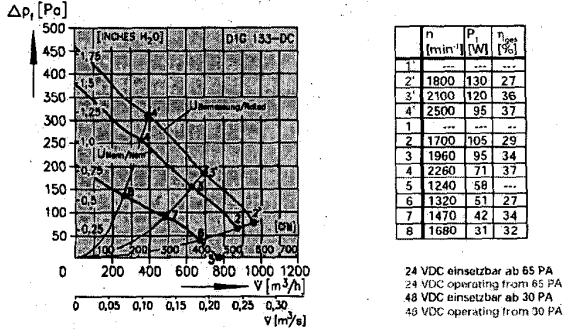


Figure 2: ebm blower-motor data

$$W_2 = W_1 \left(\frac{\omega_2}{\omega_1} \right) \quad p_2 = p_1 \left(\frac{\omega_2}{\omega_1} \right)^2 \quad (8)$$

to populate the 10 data points on four rotational speeds and fit a second order polynomial for each speed. Then we fit three forth order polynomials for each coefficient based on speed ω . The goodness of the fit is shown in Figure 3.

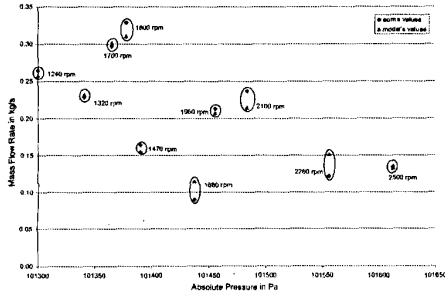


Figure 3: Data points from ebm's and model values.

For the rest of this study we use two blowers in series to double

the static pressure. It doesn't change the other characteristics and allow us to work with a larger downstream pressure.

The flow out of the supply manifold is specified by the FC flow-backpressure characteristics. We assume laminar flow:

$$W_{sm} = k_{out}(p_{sm} - p_{st}) \quad (9)$$

where p_{st} is the cathode pressure which represents the downstream pressure from the supply manifold. The nozzle constant, k_{out} , represents inverse of the flow resistance of the cathode. The value of k_{out} depends mainly on the design and the size of the air flow channels of the fuel cells. Thus, the value of k_{out} varies with different stack design.

5 Low-Pressure System Equilibria and Linearization

Ideally, a linear system of the state vector (p_{sm}, ω) is needed in order to find the eigenvalues and thus study the system transient behavior. But the system equations, especially thermodynamic equations and blower map fitting, are too complex to even find an equilibrium point for the linearization. Consideration of the operating region suggests several system simplifications.

Indeed, observation of Figure 4 shows that the blower is able to deliver a flow rate up to 0.5 kg/s whereas, the FC requires a maximum of 0.1 kg/s. Therefore, for a flow rate smaller than 0.1 kg/s we can approximate the blower flow W_{bl} with a linear relationship:

$$W_{bl} = \sum_{i=0}^1 \left(\sum_{j=0}^2 \bar{a}_{ij} \omega^j \right) p_{sm}^i \quad (10)$$

The solid line shown in Figure 4 corresponds to the FC flow-backpressure trajectory of (9) for p_{st} close to atmospheric. This trajectory is achieved during a step change in FC power and is discussed in Section 7.

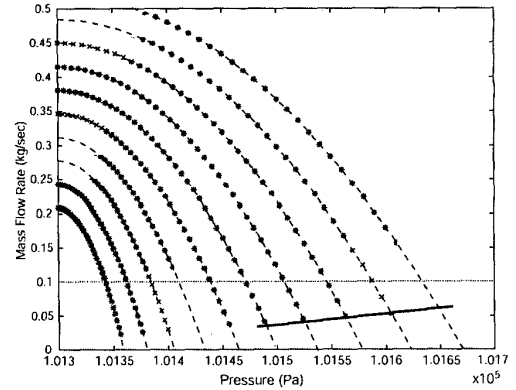


Figure 4: Blower pressure/flow map

We also simplified (5) because, in the range of pressure of our blower (101300 to 101650 Pa), the term $(p_{sm}/p_{atm})^{\frac{\gamma-1}{\gamma}} - 1$ is linear. Thus, the blower power is calculated by

$$P_{bl} = \frac{C_p T_{atm}}{\eta} (\alpha p_{sm} + \beta) W_{bl} \quad (11)$$

where $\alpha = 2.8198 \times 10^{-6}$ and $\beta = -2.8565 \times 10^{-1}$. In the high pressure case, the compressor power, P_{cp} , is calculated using Equation (5).

As mentioned above, we choose, $p_{st} = 1.016 \times 10^5$ Pa as a reasonable pressure at the cathode exit close to the return manifold and $P_m = 100$ Watts which corresponds to about 40 % of the single blower power (see Figure 2). The constant k_{out} is then treated as a parameter. Note that Equation (9) indicates that k_{out} can be viewed as a conductivity for an electrical circuit (inverse of a resistance), so a larger k_{out} corresponds to larger flow through the FC for a given back-pressure. A typical value of k_{out} for HP FC system is 0.36×10^{-5} (kg/(s·Pa)) while the value for LP FC system ranges between 0.1×10^{-3} and 25×10^{-3} (kg/(s·Pa)). The system equilibrium points $[p_{sm}^o(k_{out}), \omega^o(k_{out})]$ are then calculated by solving the two nonlinear, but largely simplified, equations (2) and (4) for $W_{bl}(=W_{fd})=W_{sm}$ and $P_m=P_{bl}(=P_{fd})$. Figure 5 shows the equilibrium points for positive values of k_{out} . It is shown

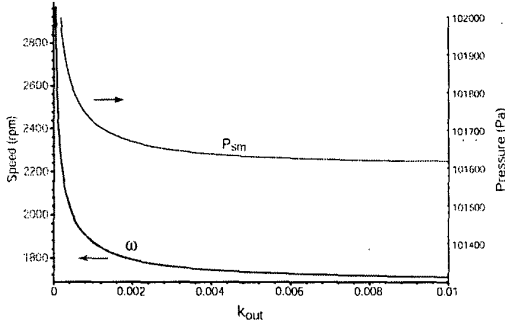


Figure 5: Equilibrium values for supply manifold pressure p_{sm} and ω as a function of k_{out} .

that as k_{out} increases p_{sm} approaches the downstream pressure p_{st} , which is logically expected when the FC lumped flow resistance decreases. In a similar manner, ω decreases as k_{out} increases.

The eigenvalues can be calculated from the linearized system:

$$\begin{bmatrix} \delta \dot{p}_{sm} \\ \delta \dot{\omega} \end{bmatrix} = M \begin{bmatrix} \delta p_{sm} \\ \delta \omega \end{bmatrix} \quad (12)$$

with

$$\begin{aligned} m_{11} &= \frac{RT}{V_{sm}} \left(\left[\frac{\partial W_{fd}}{\partial p_{sm}} \right]_{p_{sm}^o, \omega^o} - \left[\frac{\partial W_{sm}}{\partial p_{sm}} \right]_{p_{sm}^o, \omega^o} \right) \\ m_{12} &= \frac{RT}{V_{sm}} \left[\frac{\partial W_{sm}}{\partial \omega} \right]_{p_{sm}^o, \omega^o} \\ m_{21} &= -\frac{1}{J} \left[\frac{\partial \tau_{bl}}{\partial p_{sm}} \right]_{p_{sm}^o, \omega^o} \\ m_{22} &= \frac{1}{J} \left(\left[\frac{\partial \tau_m}{\partial \omega} \right]_{p_{sm}^o, \omega^o} - \left[\frac{\partial \tau_{bl}}{\partial \omega} \right]_{p_{sm}^o, \omega^o} \right) \end{aligned}$$

Both eigenvalues are negative and real for all value of k_{out} as shown in Figure 6. It means that the system is overdamped for all possible value of k_{out} . But, as we can see in Figure 6, one eigenvalue is a very large that corresponds to very fast dynamics, and the other is a very small negative number that dominates the system transient response. We see that for k_{out} from 0 to 0.005, λ_1 changes from -0.005 to -0.25 and λ_2 changes from -6000 to -30000.

The low pressure air supply subsystem (blower and manifold) has two very different eigenvalues. Based on data from an acquired low pressure FC system, $k_{out} = 0.42 \times 10^{-3}$ (kg/(s·Pa)),

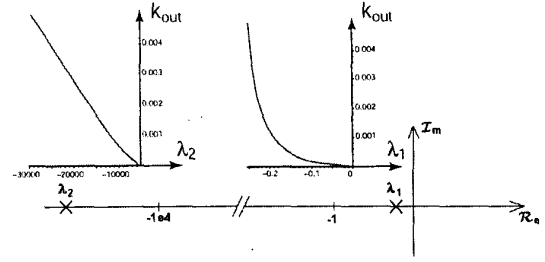


Figure 6: Eigenvalues for the LP air supply FC subsystem.

and it corresponds to eigenvalues -6035 and -0.1. Obviously, the system is composed of two subsystems which have drastically different dynamic behavior. One is very fast (eigenvalue of -6036) and the other is very slow (eigenvalue of -0.1).

6 Sensitivity on Parameters of the Air Supply Subsystem

It would be interesting to see the influence of the volume of the manifold and the blower inertia on these eigenvalues. Both the manifold volume and the blower inertia are design parameters that are typically defined by the vehicle designers and the blower manufacturers. Note that sometimes the supply manifold volume needs to be large due to the vehicle safety constraints that require the power electronics and electric motors to be separate from the hydrogen-rich environments (H_2 tank and FC stack). Their choice has implication on the dynamic system performance because the system matrix and its eigenvalues depend of these parameters. We can plot the eigenvalues of the LP as function of the inertia (keeping constant volume) and the volume (keeping constant inertia). The results are shown in Figure 7. The nominal value of V_{sm} and J are 0.02 m^3 and $5 \times 10^{-5} \text{ kg} \cdot \text{m}^2$, respectively.

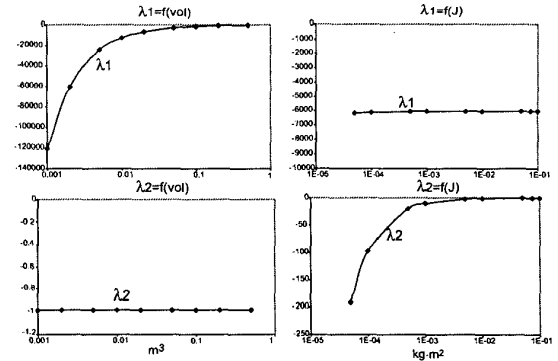


Figure 7: Influence of the Supply Manifold Volume and of the Motor Inertia on the eigenvalues (λ_1 and λ_2) of the Low Pressure System.

For the LP system, the inertia only influences the slower eigenvalue and the volume the faster eigenvalue. When the inertia decreases, the small eigenvalue increases (in absolute value). Note that the inertia does not affect the eigenvalue that correspond to the fast dynamics, but determines the dominant slow eigenvalue location. Similarly, the volume does not affect the slow dynamics but it has a large influence on the fast dynamics. We, thus, conclude that the LP second or-

der system can be decomposed to a slow "Inertia subsystem" that is determined by the blower rotational speed dynamics and a fast "Air Volume Subsystem" that is determined by the supply manifold pressure dynamics. Similarly, with practical values of volume and inertial, examination of the subspaces of each of the two eigenvectors provides corroboration for the existence of a slow (inertia) and fast (volume) subspace. For numerical (simulation with a small integration step) and analytical simplicity, one can eliminate the pressure dynamics (fast dynamics) and assume the steady-state solution of (7).

We perform the same analysis for the HP air subsystem that is based on a high speed compressor in [8]. The volume of the manifold used for the HP system is the same as the one used for the LP System : 0.02 m^3 . The HP compressor inertia ($J_{HP} = 5.10^{-5} \text{ kg}\cdot\text{m}^2$) is much smaller than the inertia of the LP blower ($J_{LP} = 0.01 \text{ kg}\cdot\text{m}^2$). For these volume and inertia values, the eigenvalues of the HP (High Pressure) system are : -23.6, -2 and -11. There are 3 eigenvalues due to the temperature variation in the supply manifold. We see that the eigenvalues of the HP system are closer to each others than for the LP System. It means that the dynamics of the states ("pressure", "speed" and "temperature") are coupled. Figure 8 shows the influence of the manifold volume and compressor inertia on the HP System. The volume and inertia affect all three eigenvalues. Thus the state space dimension cannot be reduced and remains three.

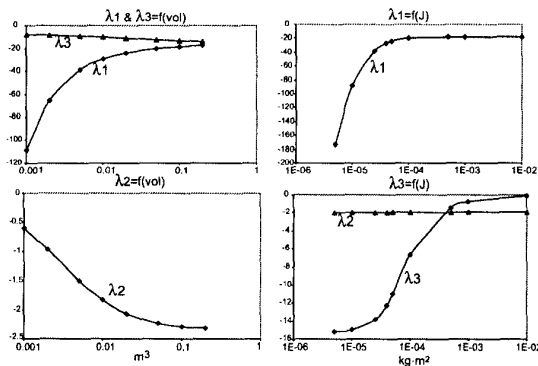


Figure 8: Influence of the Supply Manifold Volume and of the Motor Inertia on the eigenvalues of the High Pressure System.

It is important here to note that, even though the LP and the HP systems have the same manifold volume and flow rate, they have distinctly different pressure dynamics. The pressure of the LP system is a lot smaller than the one in the HP system. Moreover, the changes in pressure of the LP system are several orders of magnitude smaller than the pressure changes in the HP system during standard power steps. Pressure in the LP system remains almost constant when it is seen from the range and perspective of the high pressure system. Thus, the singularly perturbed dynamics of the LP system are physically justified. In fact when there is a step in the input of the blower motor, the pressure follows the speed to reach its final value as shown in Figure 10. It means that the system is driven by the blower inertia, and that the pressure follows the evolution of the speed very rapidly.

To have the same dynamic characteristics for the two system

(high pressure and low pressure), which means to have the same range of eigenvalues, then the inertia of the LP system has to be $0.005 \text{ kg}\cdot\text{m}^2$ (divided by 2) and the volume of the manifold 5 m^3 . Then the eigenvalues become -26 and -2, which are very close to the HP system. But such a volume for the manifold is of course not realistic. On the other hand, the value requested for the inertia is realistic and we will use that value for the rest of the study. It will be easier to compare the two systems if they have similar time constants.

7 Performance Comparison

In this section we compare the response of both high pressure and low pressure fuel cell systems to variations in power demand of an automotive application.

For all the comparative studies we are working with the whole fuel cell model (air supply, hydrogen supply, stack, etc). In the LP system, the constant of the linearized orifice equation between the cathode and the return manifold is chosen to be 200 times larger than that of the HP system, and the effective area of the exit pipe is the same.

First, we simulate a step change in power demand. We request both systems (HP and LP) to produce the same step of net power, P_{net} , (power produced by the stack - power used to drive the compressor/blower). The excess ratio of O_2 is always kept at 2. The step is from 29 kW to 38 kW (40 hp to 50 hp). In this simulation, the static feedforward map is used to find the stack current from the desired net power, $I_{st}(P_{net}^{des})$ and also to find the motor power input, based on the current, $P_m(I_{st})$, that satisfies the desired excess ratio.

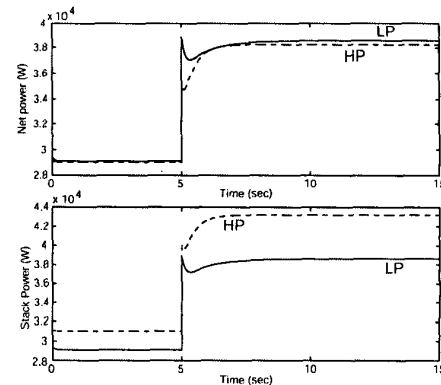


Figure 9: Net power step response for a HP and a LP FC system.

Figure 9 shows that the LP system can react a little faster than the HP system, although their slight differences can be eliminated with adequate closed loop blower controller. We also see that to obtain the same net power the HP system requires much larger power from the stack. The LP system needs less power to drive the blower than the HP system needs to drive the compressor. So at this level of net power (i) the LP system is more efficient than the HP system (ii) the LP system has a transient response similar to but a little faster than the HP system.

We can now visualize the evolution of the mass flow rate versus the static pressure for both compressor and blower. The

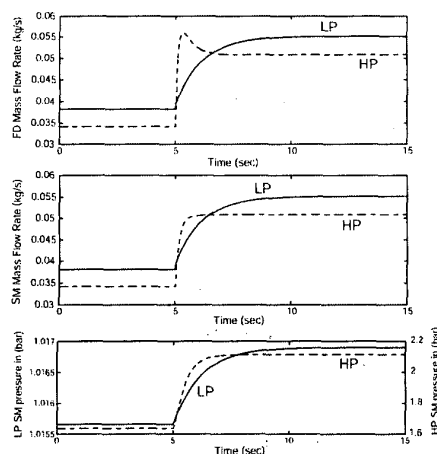


Figure 10: Pnet step : Response of the mass flow rates; upper plot shows W_{fd} lower plot shows W_{stm} .

blower is following a straight line (shown in Figure 4). On the other hand, the compressor is following an arc as shown in Figure 8 in [9] with the compressor flow growing first and a lot faster than the pressure.

In Figure 11, we show the polarization curves of the cells for both systems subjected to a ramp current demand. This is the FC voltage as a function of the current drawn in one cell when blower and compressor sustain the same excess oxygen ratio (λ_{O_2}). We see that the LP system is not able to keep the same values of voltage in the cells as the HP system. So, in terms of the use of the fuel cell full potential, the LP system is less efficient.

Figure 12 shows the net power of the LP and the HP system for different current levels. In automotive applications there is a need for more investigation on the matching of these electrical and power characteristics with an appropriate traction motor and a DC/DC converter. The power-current characteristics indicate the need for a better match between the LP FC and the flow. The low pressure fuel cell "engine" would develop much less power than the high pressure one and be limited at 40 kW while the HP system's stack can produce 75 kW [9]. On the other hand, the low pressure fuel cells system is lighter, has the potential for faster response, and might be more reliable than the high pressure system. There is a compromise to find.

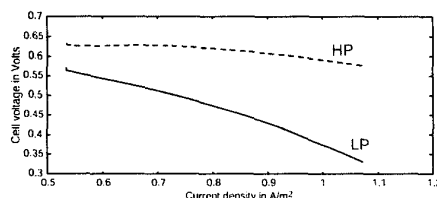


Figure 11: Polarization curves of the cells for LP and HP Systems.

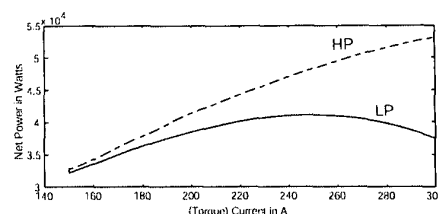


Figure 12: Net Power vs Current for LP and HP Systems.

8 Concluding Remarks

This paper provides a dynamics engineering perspective on the issue of FC operating pressure. It complements a significant body of work on the relative merits and difficulties between the two systems. It is anticipated that this perspective will provide insight on the system dynamics and the control implementation of FC based powertrains.

References

- [1] F. Barbir, M. Fuchs, A. Husar, and J. Neutzler. Design and operational characteristics of automotive PEM fuel cell stacks. *SAE Paper 2000-01-0011*.
- [2] J.M. Cunningham, M.A. Hoffman, and D.J. Friedman. A comparison of high-pressure and low-pressure operation of PEM fuel cell systems. *SAE Paper 2001-01-0538*.
- [3] J.M. Cunningham, M.A. Hoffman, R.M. Moore, and D.J. Friedman. Requirements for a flexible and realistic air supply model for incorporation into a fuel cell vehicle (FCV) system simulation. *SAE Paper 1999-01-2912*.
- [4] Argonne National Laboratory. *GCTool Help Documentation*.
- [5] James Larminie and Andrew Dicks. *Fuel Cell Systems Explained*. John Wiley & Sons Inc, West Sussex, England, 2000.
- [6] P. Moraal and I. Kolmanovsky. Turbocharger modeling for automotive control applications. *SAE Paper 1999-01-0908*.
- [7] S. Pischinger, C. Schönfelder, W. Bornscheuer, H. Kindl, and A. Wiartalla. Integrated air supply and humidification concepts for fuel cell systems. *SAE Paper 2001-01-0233*.
- [8] J.T. Pukrushpan, H. Peng, and A.G. Stefanopoulou. Simulation and analysis of transient fuel cell system performance based on a dynamic reactant flow model. *Proceedings of the ASME International Mechanical Engineering Congress & Exposition*, 2002.
- [9] J.T. Pukrushpan, A.G. Stefanopoulou, and H. Peng. Modeling and control issues of PEM fuel cell stack system. *Proceedings of the 2002 American Control Conference*, pages 3117–3122, 2002.
- [10] A. Wiartalla, S. Pischinger, W. Bornscheuer, K. Fieweger, and J. Ogrzewalla. Compressor expander units for fuel cell systems. *SAE Paper 2000-01-0380*.